Abstract: 397
Manuscript: 5735
Figures: 9
Supplemental Information: 5

Energy in functional brain states correlates with cognition in adolescent schizophrenia and healthy persons

Nicholas Theis[1§]

Jyotika Bahuguna[2§]

Jonathan E. Rubin[3]

Brendan R. Muldoon[1]

Konasale M. Prasad[1,4,5*]

[1]Department of Psychiatry, University of Pittsburgh School of Medicine, Pittsburgh, PA, USA

[2]Department of Psychology, Carnegie Mellon University, Pittsburgh, PA, USA

[3]Department of Mathematics, University of Pittsburgh, PA, USA

[4]Department of Bioengineering, Swanson School of Engineering, University of Pittsburgh, PA, USA

[5]Veterans Affairs Pittsburgh Healthcare System, Pittsburgh, PA, USA

§Equally contributed

***Corresponding author:**

3811 O'Hara Street, Pittsburgh, PA 15213, USA; KMP8@pitt.edu

Abstract

Adolescent-onset schizophrenia (AOS) is a relatively rare and under-studied form of schizophrenia with more severe cognitive impairments and poorer outcome compared to adult-onset schizophrenia. Several neuroimaging studies have reported alterations in regional activations that account for activity in individual regions (first-order model) and functional connectivity that reveals pairwise co-activations (second-order model) in AOS compared to controls. The pairwise maximum entropy model, also called the Ising model, can integrate both first-order and second-order terms to elucidate a comprehensive picture of neural dynamics and captures both individual and pairwise activity measures into a single quantity known as energy, which is inversely related to the probability of state occurrence. We applied the MEM framework to task functional MRI data collected on 23 AOS individuals in comparison with 53 healthy control subjects while performing the Penn Conditional Exclusion Test (PCET), which measures executive function that has been repeatedly shown to be more impaired in AOS compared to adult-onset schizophrenia. Accuracy of PCET performance was significantly reduced among AOS compared to controls as expected. Average cumulative energy achieved for a participant over the course of the fMRI negatively correlated with task performance, and the association was stronger than any first-order associations. The AOS subjects spent more time in higher energy states that represent lower probability of occurrence and were associated with impaired executive function suggesting that the neural dynamics may be less efficient compared to controls who spent more time in lower energy states occurring with higher probability and hence are more stable and efficient. The energy landscapes in both conditions featured attractors that corresponded to two distinct subnetworks, namely fronto-temporal and parieto-motor. Attractor basins were larger in the controls than in AOS; moreover, fronto-temporal basin size was significantly correlated with cognitive performance in controls but not among the AOS. The single trial trajectories for the AOS group also showed higher variability in concordance with shallow attractor basins among AOS. These findings suggest that the neural dynamics of AOS features more frequent occurrence of less probable states with narrower attractors, which lack the relation to executive function associated with attractors in control subjects suggesting a diminished capacity of AOS to generate task-effective brain states.

Keywords: Adolescent onset schizophrenia; Executive function; Maximum Entropy Model; Energy landscape analysis; Attractors; Cognitive impairments

1. Introduction

Adolescent onset schizophrenia (AOS) has phenomenological continuity with adult-onset schizophrenia[1-3] yet is associated with more prominent developmental and premorbid abnormalities. Hence, AOS is proposed as a more severe form of schizophrenia[4] with more severe cognitive impairments[1,3,5-7], especially in working memory[8-11], executive functions[1,3,6,7], and attention[5,7,12,13], and with poorer long-term outcomes[1-4]. Cognitive deficits respond minimally to antipsychotics[14,15] and are consistently associated with poor long-term outcome[16-19]. Further, AOS is under-investigated than adult-onset schizophrenia. A better understanding of the pathophysiology of AOS could enable novel treatment strategies to improve outcomes.

Among several approaches available to investigate the pathophysiology of schizophrenia, functional magnetic resonance imaging (fMRI) offers the advantage of examining blood oxygenation level dependent (BOLD) responses as proxy measures of brain activation. Currently, most fMRI studies have examined group differences in the activation of brain regions, namely first-order models[20], or pairwise correlations of spatially distributed regions and derived functional networks based on co-activations, namely second-order models. These approaches have highlighted distinct aspects of brain functioning at rest and while performing cognitive tasks[21,22]. These models provide limited information at the systems level. For example, first-order-only analyses cannot elucidate detailed system-level interactions among regions while second-order models do not provide information about regional activation differences and often do not provide mechanistic insights.

Alternatively, energy models mathematically integrate both the first-order and second-order dynamics among brain regions[23] in a way that relates to the empirical occurrence probabilities of states. One such model is the pairwise maximum entropy model (MEM)[23,24], an inverse Ising inference tool[25], which can represent fundamental properties of the brain: distant regions interact according to an underlying network configuration to produce brain states of varying likelihood. The Ising model treats regions as two-state (binary) nodes. Network structure (*J*) and nodal importance (*h*) in the MEM together capture the frequency of occurrence of discrete state configurations across all nodes. The term "energy" in this setting does not refer to physical energy (in joules) nor to metabolic energy (as adenosine triphosphate) but is used in the mathematical context of the model, where energy is inversely related to probability, with higher energy associated with low probability states. This energy term is more specifically referred to as the "integrated energy" of the system configuration when applied to fMRI data[26.] It provides a representation of time-specific regional brain activation or inactivation while also accounting for the system's connectivity and pairwise interactions in terms of correlated activations of regions. Energy and cognitive performance may be related[27,] suggesting that this energy term reflects the complexity of the mental work being done or the efficiency of strategies adopted to complete a cognitive task.

Although the MEM approach was originally used in physics to model magnetic fields[28], versions of the MEM have more recently been used in studies associated with cognitive functions . The MEM approach is especially useful to investigate time-varying dynamics during cognitive tasks because the model includes BOLD responses at every repetition time (TR) of the fMRI acquisition[27]. Further, investigation of brain networks using a pairwise MEM and associated energy landscape provides a useful model of principles of network organization that can then be compared between different states of the

networks or across subject groups. A prior study showed a high number of local minima in a resting fMRI suggesting that in rest conditions, the brain naturally reverts to one of a collection of preferred states[29]. Experimentally induced perturbations reduced the number of local minima considerably, while other effects depended on the specifics of the perturbation[30]. Another resting fMRI study showed different characteristics of the energy landscape in the default mode and frontoparietal networks[31]. In this work, we provide what is to our knowledge the first study to apply the MEM model to elucidate complex network dynamics in AOS or adult-onset schizophrenia patients using fMRI data.

Task-fMRI can provide data on differences in functional and network characteristics that can be used as biomarkers and as treatment targets. Previous studies have reported impaired executive function in AOS[1,3,7] and adult-onset schizophrenia[32-35] patients. We selected the Penn Conditional Exclusion Test (PCET) as an fMRI task to test executive function, which is a part of the Penn Computerized Neurocognitive Battery that has been validated in schizophrenia[36] and healthy[37] subjects and used in our previous studies[38-41]. PCET is closely related to the Wisconsin card sorting test and to verbal fluency and work behavior such as cooperativeness, work quality, and general impressions including quality of work, verbal fluency and executive function[42].

Here, we applied the pairwise MEM to fMRI data obtained while participants were performing the PCET task. The MEM model (**Figure 1**) was iteratively fit to the entire set of observed brain states, using their empirical probabilities to estimate unknown parameters in the MEM. The relationship between MEM energy and cognitive performance assessed as accuracy of in-scanner PCET was examined. We hypothesized that the average energy attained by an individual over the course of the experiment is related to PCET accuracy and that the relationship will be stronger than correlation with first-order activation. In addition to supporting these hypotheses, our results show that the AOS and controls visit states at different frequencies, with the AOS group spending more time in higher energy states.

2. Methods

2.1. Sample description

We enrolled 23 AOS from in- and out-patient clinics of the University of Pittsburgh Medical Center, Pittsburgh and 53 adolescent healthy controls from the community. Adolescent-onset was defined as schizophrenia subjects who had an onset of psychotic symptoms after puberty but before completing the age of 18 years. Puberty was assessed using the Peterson Pubertal Developmental Scale and all subjects had to score ≥2 to be eligible for enrolment. Participants diagnosed with intellectual disability according to the DSM-IV, having history of substance use disorder in the last 3 months, head injury with significant loss of consciousness, tumors, encephalitis, and had suffered neonatal asphyxia were excluded. Subjects were administered the Structured Clinical Interview for DSM-IV (SCID-IV) and selected items on the Kiddie-Schedules for Assessment of Depression and Schizophrenia (K-SADS). Consensus diagnosis by experienced clinical investigators was made after reviewing all available clinical data including the charts. The University of Pittsburgh Institutional Review Board approved the study. Informed consent was obtained from all participants after providing a full description of the study including the risks and benefits. Controls

were 18.9±1.76 years old and 51% female, and AOS were 19.7±1.14 years old and 68% female. HC were significantly younger than AOS (t=2.04; p=0.045) but sex distribution was not statistically different between the groups (χ^2=1.86 p=0.17).

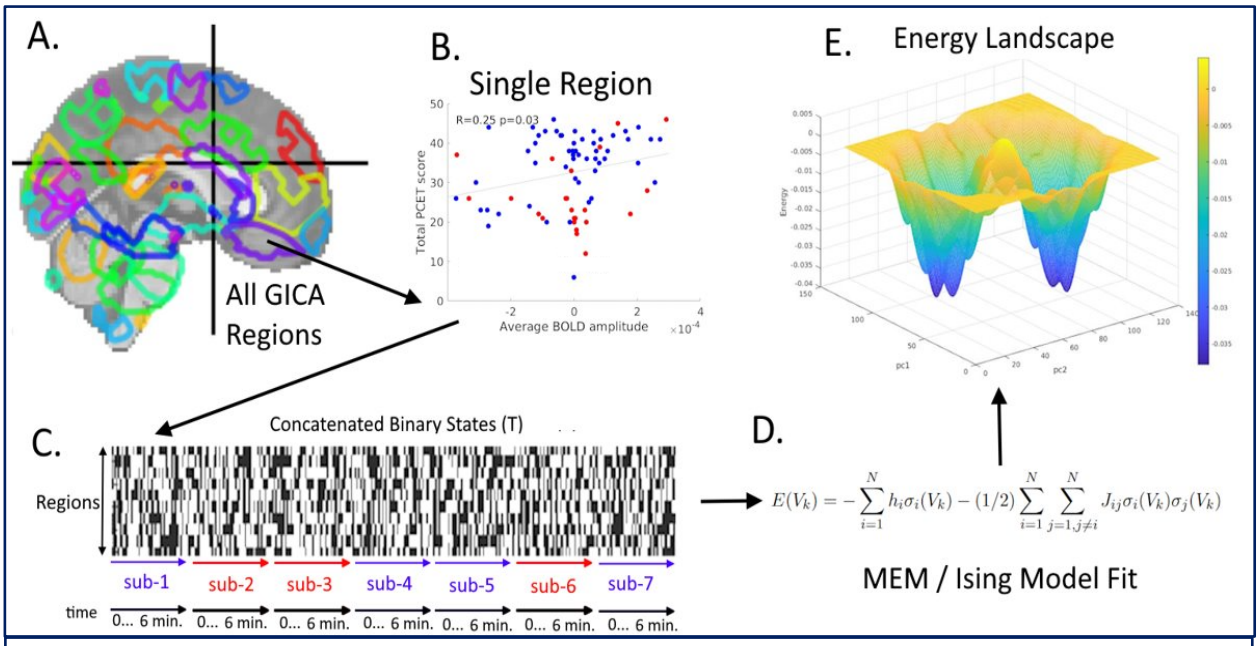

Figure 1: Methodological Outline. The minimally preprocessed fMRI data is further processed using group independent component analysis (GICA) to find 70 components (A). For each of the 70 components, the correlation of mean individual-level BOLD signal amplitude with performance on PCET is computed (B) and the regions with nominally significant correlation of BOLD responses to PCET performance are selected (n=9 regions). Blue points are controls; red points are AOS subjects. The temporal activity series of these 9 regions are then binarized at the individual level and concatenated together across all individuals in the study (C), creating the concatenated binary matrix, T. The maximum entropy model (D) is then fit to this matrix. The resulting energy term can be represented in a number of ways, including in terms of principal components (from performing PCA on T), which in particular produces an energy landscape (E). Legend: sub=subjects

2.2. Image Acquisition and Preprocessing

T_1-weighted MP2RAGE scans were acquired in the axial plane (348 slices, 0.55 mm thickness, TE=2.54ms, TR=6 seconds, in-plane resolution=390x390). Functional MRI echo-planar images were acquired in the axial plane (86 slices, 1.5 mm thickness, TE=20ms, TR=3 seconds, in-plane resolution=148x148, 142 volumes). fMRI data was collected while subjects performed the PCET task. Our choice of PCET performance is supported by previous studies that relate executive function to workplace behavior[41]. These domains are impacted by schizophrenia. Each trial presented four shapes and participants selected the shape that did not belong. The sorting principles changed, with feedback to help subjects develop new strategies. Subjects were expected to select the correct stimulus with the minimum number of errors despite changing sorting principles. Such set shifting was considered to indicate cognitive flexibility, which is subsumed as executive function[42]. The number of correct responses was counted as the measure of accuracy of performance.

All the pre-processing steps for the fMRI data were performed using fMRIPrep[43], which included correction for motion, slice timing, bias, and distortion, and brain extraction before registering to a standard space (MNI 152) using the Human Connectome Project approach[44]. Image registration of fMRI volumes to standard space was performed using co-registration with the T_1-weighted image.

2.3. Region Selection

Group Independent Component Analysis (GICA) was used to define spatial maps[45]. This allowed us to focus on task driven BOLD signals that appear on the inter-subject level[46]. GICA is performed using a larger selection of components than expected to be necessary to explain the task-associated regions. Here, we chose 70 components[47].

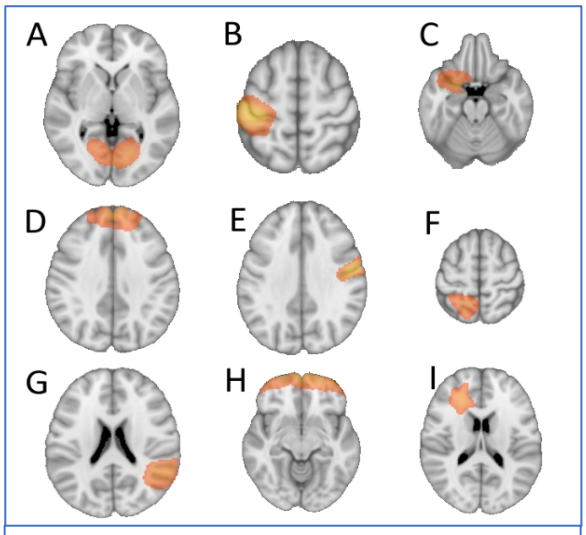

Figure 2: Spatial representations of the 9 selected brain regions from GICA. The regions roughly correspond to the following anatomical areas: A) calcarine, B) left precentral, C) left olfactory, D) frontal superior medial, E) right postcentral, F) left parietal superior, G) right temporal superior, H) frontal superior orbital, and I) a region labeled as white matter/no label which is located near the left anterior cingulate.

We selected a subset of *N* components that showed nominally significant correlation of BOLD responses to the performance on PCET for inclusion in the energy model **(Figure 2)** because careful selection of regions could contribute to the effectiveness of the model. The region selection step was purely data-driven to choose informative timeseries for the energy model and to enhance computational tractability through an exponential downscaling of the number of possible states included in the energy computation[48]. The white matter region was included despite the unorthodoxy of white-matter-derived BOLD signals[49] (see discussion).

2.4. Concatenation and Binarization

After selecting the regions, all observations were binarized, and then timepoints across all subjects were concatenated together in a matrix *T* with *N* rows representing regions and a number of columns, *M*, equal to the total number of timepoints (TR) in the entire sample, across all subjects. That is, we assume that each subject has the same number of timepoints, *p*, and take $M=S*p$ where *S* denotes the number of subjects. The concatenated state matrix, *T*, must be binary, and so the components are binarized. The threshold choice for binarization can affect the outcome of the energy model (**Figure 3**).

The seven threshold choices tested for binarizing the independent components (ICs, which are BOLD-derived and z-scored) at a given moment in time, a given region, and a given subject (more succinctly, a "microstate") are 0, +/- 0.5, +/- 1.0, and +/- 2.0. The middle or threshold 0, where roughly half of all microstates are in the "on" position across all subjects and timepoints, was chosen because it

produced the most informative energy landscape (see Section 2.5) with the best fit of the energy function to the empirical probabilities of state occurrence. All data in this manuscript uses this threshold.

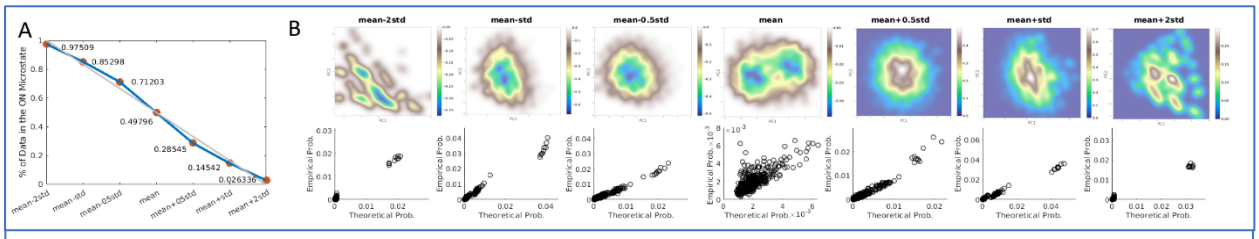

Figure 3: Threshold Effect on Energy. Left: The percent of data in the 'on' microstate across all subjects and timepoints after thresholding. Right: Seven thresholds were tested (x-axis), namely mean minus two standard deviations, mean minus one standard deviation, mean minus one-half standard deviation, mean, mean plus one-half standard deviation, mean plus one standard deviation, and mean plus two standard deviations. The middle threshold (mean) was chosen because in the threshold sweep results to the right, mean yielded the most complete "energy landscape" (top row, middle plot), and best fit of the empirical probabilities of state occurrence (bottom row, middle plot).

2.5. Energy Model

Energy, E, is defined for each possible binary state, V_k, according to the Ising model[23] as:

$$E(V_k) = -\sum_{i=1}^{N} h_i \sigma_i(V_k) - \left(\frac{1}{2}\right) \sum_{i=1}^{N} \sum_{j=1.j\neq i}^{N} J_{ij} \sigma_i(V_k) \sigma_j(V_k) \tag{1}$$

where N is the number of regions, k indexes the state from among the B possible unique binary states where $B=2^N$, J is the 2-dimensional adjacency matrix that defines the coupling of region pairs, and h is the vector of activation parameters. The parameters are fit using a maximum entropy approach. For each index k, V_k is a vector with N elements, $V_k = [\sigma_{k1}, \sigma_{k2}, \ldots, \sigma_{kN}]$, where each element σ_{ij} (the binary value for a given region at a given state) can be either 1 or 0. The set of all *possible* unique binary states is defined as: $V=[V_1, V_2, \ldots, V_B]$. This is not to be confused with T, which concatenates all *observed* binary states and may feature the same configuration appearing in multiple columns.

While the energy value itself has no absolute interpretation and only relative changes in energy are meaningful, state energy maps to state probability, $P(V_k)$, as follows:

$$P(V_k) = exp\left(-E(V_k)\right) / \sum_{i=1}^{2^N} exp\left(-E(V_i)\right). \tag{2}$$

The values of h_i and J_{ij} in equation (1) were iteratively estimated by comparing the actual and estimated values of mean and covariance between the nuclei and adjusting them with learning rate α (0.2). Specifically, we calculated the estimated mean and covariance and performed the iterations of h_i and J_{ij} as follows:

$$\langle \sigma_j \rangle_m = \sum_{q=1}^{2^N} \sigma_j(V_q) P(V_q)$$

$$\langle \sigma_j \sigma_l \rangle_m = \sum_{q=1}^{2^N} \sigma_j(V_q)\sigma_l(V_q)P(V_q)$$

$$h_i^{new} = h_i^{old} + \alpha \cdot log\left(\frac{\langle \sigma_i \rangle}{\langle \sigma_i \rangle_m}\right)$$

$$J_{ij}^{new} = J_{ij}^{old} + \alpha \cdot log\left(\frac{\langle \sigma_{ij} \rangle}{\langle \sigma_{ij} \rangle_m}\right)$$

We ran 300 iterations of the gradient descent algorithm and that resulted in a good fit between the first-order (mean activity) and second-order (co-activation) statistics (see Section 2.6).

We also fitted separate MEM to the data corresponding to the control group and to the AOS group separately using the same procedure that was described for the combined data. The implementation of the MEM in Python is available on GitHub, along with functions used for energy landscape visualizations (https://github.com/theisn/IsingModel_fMRI/tree/master).

2.6. Evaluating Fit of the Model

We evaluated the fit of the model by comparing the estimated and actual first-order (mean) and second-order (covariance) features of the data **(Supplemental Figure 1)**. As an additional check, we also examined the relationship between the energy and probability of occurrence of each state as estimated by the model and the empirical probability of each state in the data, which also demonstrated a good fit (**Supplementary Figure 2**). We also ensured that there were more observations than the entropy of the system (in bits). Specifically, the state space size (given by *B*) refers to the number of *N* x 1 vectors of binary regional activity, across all subjects and timepoints. In this case, *N*=9, so $B=2^N=512$. The number of observations refers to the number of columns in *T*, which here is 10,792 (approximately twenty times *B*), justifying that we had an adequate sample for implementing the MEM.

2.7. Energy Landscape via Projection onto Principal Components

From equation (1), we derived a vector of energy values along a sequence of time points for each subject. While essential, the time and energy dimensions do not tell the full story. Since the basis for the energy value is the *N*-dimensional brain state configuration, and time points with the same energy value could correspond to very different brain states, we used Principal Component Analysis (PCA), performed on *T*, the matrix of observed binary states concatenated across all subjects and time points, to describe states in terms of a lower-dimensional manifold.

The PCA isolates the orthogonal eigenvectors that explain the most variance in the data. Our aim was to visualize an energy landscape in the state space of eigenvectors of the data, where two dimensions represent the data projected onto the first 2 principal components (PCs) and the 3rd dimension represents the energy corresponding to the state. The energy landscape was smoothed with a 2-dimensional

Gaussian kernel, with σ=1.5; in brief, the smoothing process introduces a kernel centered at each data point and computes a smooth function by summing over these kernels. The smoothed version was used to visualize the energy manifolds, but all quantification was done on the individual states of the MEM. The same value of σ was used to generate all energy landscapes. The basins of attraction of energy minima correspond to low (usually negative) energy values represented with cooler colors, whereas the peaks correspond to higher (usually positive) energy values represented with warmer colors. PCA was also used to identify two sub-networks corresponding to the basins observed in the energy landscape. The loading weights of the first two PCs were thresholded (threshold=0.3) to identify the states that corresponded to "fronto-temporal" and "parieto-motor" networks. Fronto-temporal states were defined as states where frontal-superior-medial, olfactory, frontal-superior-orbital and temporal-superior were simultaneously active, whereas parieto-motor states were defined as states where post-central, precentral, parietal-superior and region corresponding to white matter were simultaneously active. The binary numerals are converted to base 10 for ease of collation, (e.g., 000000100 is state number 4).

For the MEM for the separate control and AOS data sets, the PCs were calculated separately on each group, before the corresponding data was projected on the PCs for that group.

2.8. Cognitive and Clinical Statistical Comparisons

Energy from the model was compared between AOS and healthy controls and to the cognitive performance in each clinical group. Subject-level energy scores, computed as the sum of the energies of all states over the entire course of their fMRI, were compared, using whole-group and within-group correlations, to PCET accuracy scores. The 512 states were also binned into 16 equal bins according to energy percentiles. Explicitly, 32 states (6.25% of all states) were classified into the lowest energy bin, 32 into the next-lowest energy bin, and so on. Then, the number of states experienced per energy bin was tallied by group and divided by the total number of states attained, yielding the frequency of occurrence by energy bin. The frequency of occurrence of bins in the bottom half (eight) of all energy bins were compared between AOS and controls using a Wilcoxon rank-sum test, as were frequencies for the top eight bins. A two sample Kolmogorov–Smirnov test was used to determine if the distributions of energy bins attained over time differed between groups.

2.9 Single trial trajectories

The PCET task consisted of 6 task blocks of 22 TRs (3 secs each) that were averaged for each participant to obtain their trajectory. The trajectories were smoothened using a box car kernel of length 5. The top 5 performers from the control and poorest performers on the AOS group were chosen on the basis of the 5 highest or lowest PCET scores. The ellipsoid was calculated by finding the average standard deviation across X (PC1), Y (PC2) and z (Energy) axes corresponding to the AOS and control trajectories.

3. Results

3.1 Activity in a subset of selected regions shows a significant correlation with cognitive performance

From 70 GICA components representing 92 non-contiguous regions, 9 regions (Figure 2) were found to have an average activity at the individual level that significantly correlated with the PCET total score across all participants **(Figure 4A)**, without correction for multiple comparisons. The nine regions have their components' peak voxels in the following approximate locations in the brain: left calcarine ($r=0.23$, $p<0.05$), left precentral ($r=0.23$, $p<0.05$), left olfactory ($r=0.25$, $p<0.05$), left frontal superior medial ($r=-0.25$, $p<0.05$), right postcentral ($r=-0.31$, $p<0.05$), left parietal superior ($r=-0.25$, $p<0.05$), right temporal superior ($r=0.25$, $p<0.05$), left frontal superior orbital ($r=-0.23$, $p<0.05$), and a region labeled as white matter, located near the left anterior cingulate ($r=0.30$, $p<0.05$).

3.2. Controls score higher on PCET task as compared to AOS group

Healthy controls showed significantly higher accuracy (35.1±8.4) on the PCET task compared to the AOS group (26.4±8.9) ($t=4.0$, $p<0.001$) **(Figure 4B)**.

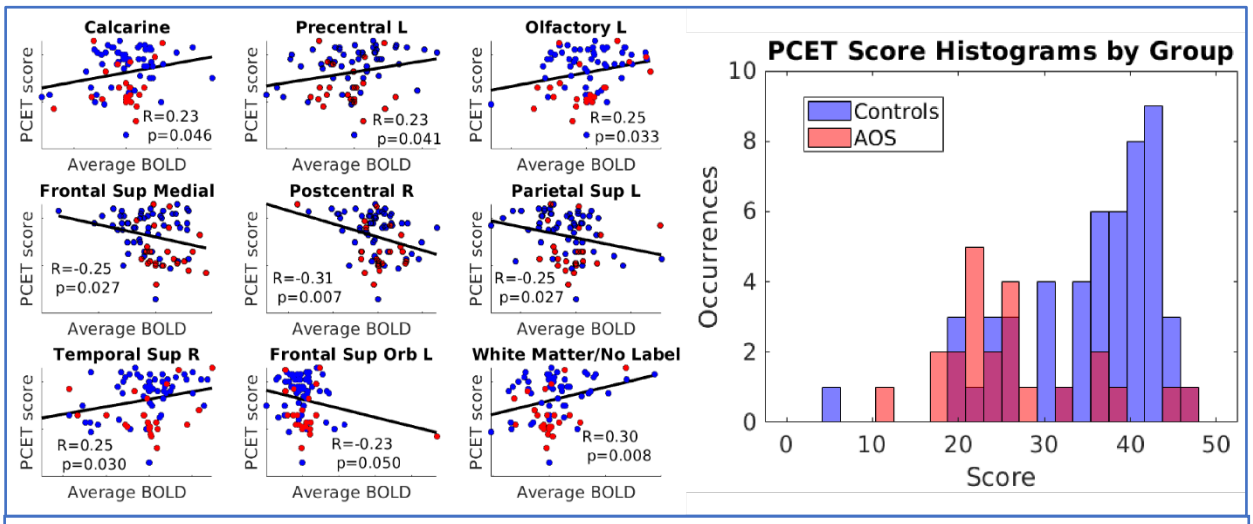

Figure 4: Region Selection and PCET scores. A) For all 70 components from GICA, each subject's average BOLD signal intensity in that component was plotted against PCET score. The X-axis in each plot is the average z-scored BOLD amplitude-derived component value. The y-axes are the PCET scores. Blue points are healthy control individuals. Red points are AOS individuals. The relationship of BOLD signals was complex in that not all regions showed positive correlation of BOLD signal with PCET performance. Notably, frontal, and parietal regions showed negative correlations. B) PCET score Histograms by group. Controls show a clear right shift in the number of occurrences of higher PCET accuracy compared to patients who mostly concentrated to the left. Blue: controls. Red: AOS. X-axis is total PCET correct. Y-axis is the number of participants in the group who scored the corresponding amount.

3.3. Average energy in MEM shows significant negative correlation with cognitive scores

We fitted an MEM to the combined data of fMRI activity from controls and AOS patients (goodness-of-fit shown in **Supplemental figure 1**). The energy landscape obtained from projecting the data onto the first two PCs of the matrix of activation states observed in all subjects (see Section 2), with energy as the third dimension, is shown in Figure 5A. The energy landscape features two primary

attractors in the activity (142 time-points per subject) dynamics during the task, each with a sizeable attraction basin (low energy areas in blue).

The average energy values across the time series of activation states for each subject were not statistically significantly different between AOS and controls (Figure 5B inset) despite the groups' clear differences in the PCET scores (Figure 4B). However, we found that the average energy value negatively correlated with PCET accuracy (Figure 5B). This relation holds both at the combined group level (N=76, r=– 0.39, p=0.0004) and separately for the control group (N=53, r=–0.30, p=0.03) and AOS (N=23, r=–0.49, p=0.019), as shown in **Figure 5B**. Thus, our results suggest that the lower average energies are correlated with higher cognitive scores for both clinical groups, suggesting that more substantial attractor basins are associated with better cognitive performance.

3.4 Controls experience more low energy states whereas AOS experience more high energy states

Although the groups' overall average energy levels do not show a significant difference **(Figure 5B-inset)**, the structure of how average (across subjects) energy varies over time (KS-stat=0.25, p=0.0035) was significantly different between groups. Moreover, the detailed structure of the activity states and their corresponding energies shows a clear difference between the clinical groups.

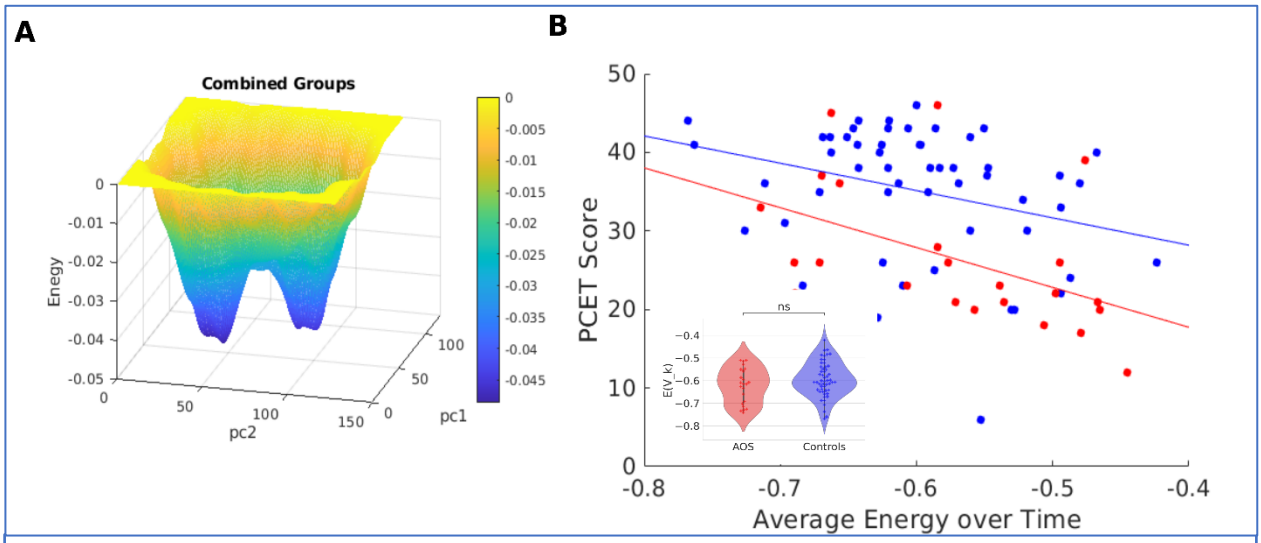

Figure 5: Average Energy versus PCET Score. A) Energy landscape of the combined model. Basins represent more negative energy (cooler colors) and peaks represent more elevated energy (warmer colors). B) The energy values averaged across the entire duration of the fMRI (142 timepoints) for each subject (Blue point: healthy controls; Red points: AOS) show significant negative correlation with PCET scores. Average energy distributions do not show statistical significance between the groups (inset).

When activation states were classified into sixteen equally sized energy bins, states in the lower half of the distribution occur with higher frequency in the controls' time series while the time series of AOS consistently included higher frequencies of states in the upper half of the energy distribution **(Figure 6A).** The Wilcoxon rank-sum test, paired on energy bins, showed significant differences in the occurrence frequencies of the lower energy states (p<0.01, signed rank=36) and higher energy states (p<0.01, signed rank=0). When individual states were compared for differences in occurrence frequency by group without

regard to their energies there were no specific, individual states with significantly different occurrence frequency by group after correction for multiple comparisons using false discovery rate.

When the binary states were ignored and the energy bins (which include multiple states) were examined over time **(Figure 6B),** the AOS group consistently achieved some of the highest energy states

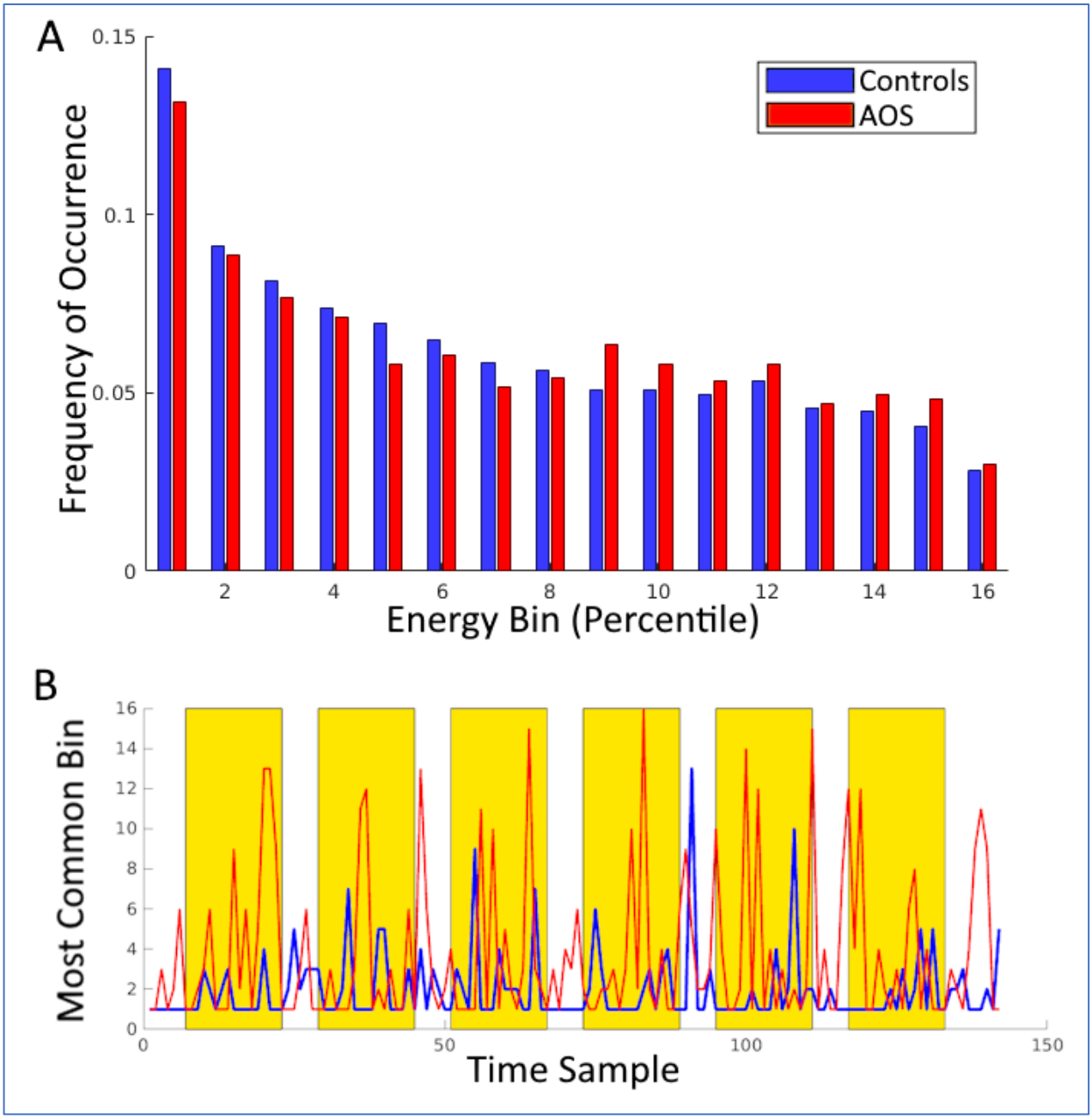

Figure 6: Controls experienced more low-energy states compared to AOS. A) Using 16 equally sized bins to cluster states based on energy percentiles, we observed that the control group experienced more low energy states and that the AOS group experienced more high energy states. Bin heights within a group sum to 1 across all bins. B) The energy level of the most frequent (modal) energy bin in each subgroup: blue is the control group (N=53) and red is the AOS group (N=23). Time samples are fMRI TR, which are 3 seconds in duration. The yellow regions represent the task blocks, which contain 8 stimuli each. Stimuli are presented every 9 seconds.

during task blocks. The high energy states during the task occurred at significantly higher frequency for the AOS group than for controls, based on a two-sample Kolmogorov-Smirnov test for distributions of the most frequent (mode) energy bins during task blocks by group (KS-stat=0.20, p=0.0034); mean energy bin during task blocks by group (KS-stat=0.24, p=0.0057) were also significantly different across groups, while the standard deviations were not different by group (**Supplemental Figure 4**).

3.5 Energy basins correspond to distinct subnetworks: fronto-temporal and parieto-motor

We further investigated the composition of the two basins we observed in the energy landscape **(Figure 5A)**. In order to compare the energy landscapes and the basin features for the clinical groups, we fitted separate groupwise MEMs to the control and AOS data (see section 2.7). The presence of the two basins was consistent even in groupwise models **(Figure 7A)**.

Analysis of the separate groupwise models showed that for AOS patients, there was a 32.94% reduction in the basin areas, calculated as area under the energy cumulative distribution function (CDF) for those energy levels less than —1.2, which we defined as the basin boundary (**Figure 7B**). This result

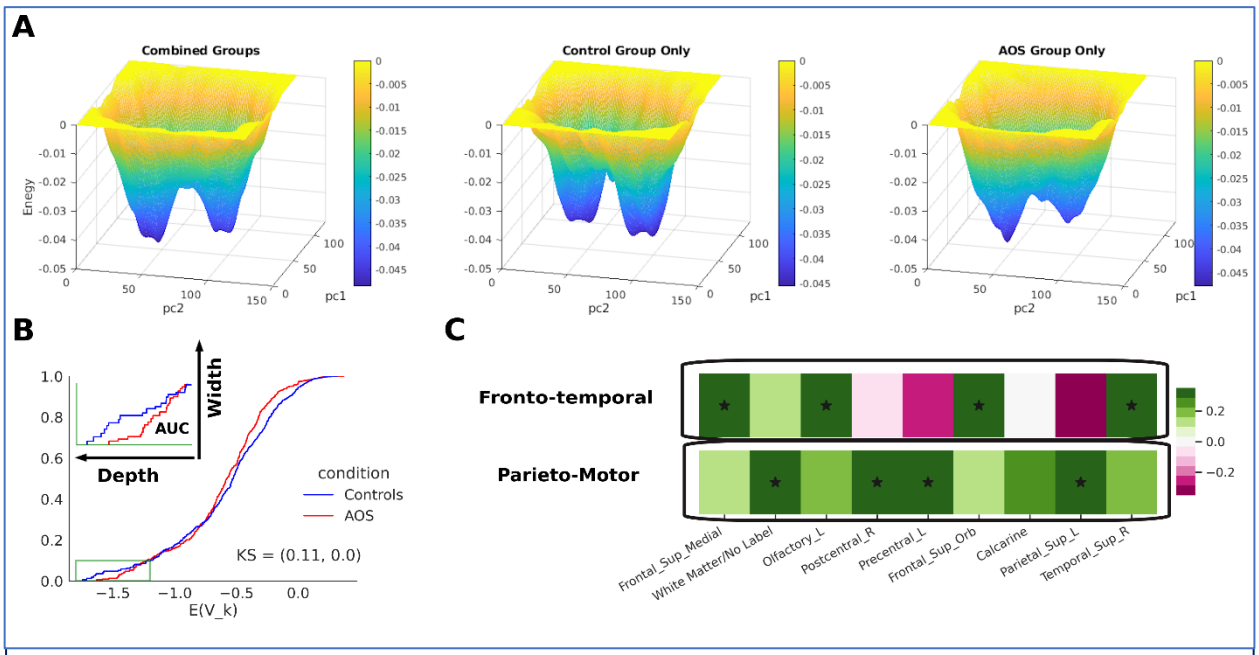

Figure 7: Energy basins correspond to distinct sub-networks. A) Comparison of energy landscapes for combined model (left) versus separate models for controls (middle) and AOS patients (right). All three manifolds show two primary basins, although the basin depths and energy barrier between basins differ across them. Basins (blue regions) represent more probable, lower energy conglomerates of states. Theoretically, an individual's brain activation states yield a sequence of positions on the energy landscape during cognition. B) Comparison of the basin areas between MEM of controls versus AOS. The area under the curve (AUC) was calculated for energy cumulative distribution functions (CDF) based on energy values less than -1.2. The lowest value of the energy CDF in a bin represents the bin *depth* and proportion of states that lie in that energy bin represents the bin *width.* The total basin AUC for AOS was 32.94% lower than for the control conditions. C) Principal component analysis over the data shows that these basins represent two distinct sub-networks, I.e., "Fronto-temporal" (Frontal-superior-medial, Olfactory, Frontal-superior-orbital, and temporal-superior regions) and "Parieto-Motor" (White matter, Post-central, Pre-central and parietal-superior regions).

aligns with our previous analysis showing that controls experienced more states in lower energy bins compared to AOS patients.

We further explored if these basins corresponded to distinct sub-networks among the areas used for fitting the model. PCA (Methods section 2.8) showed that each of the first 2 PCs explains around same amount of variance (PC1: 17%, PC2: 14%) and that the loading weights associated with these two PCs **(Figure 8)** comprise two distinct sub-networks. The first PC corresponds to a "fronto-temporal" subnetwork that consists of states that show high (above mean) activity in frontal superior medial, olfactory, frontal superior orbital, and superior temporal areas. The second PC corresponds to a "parieto-motor" subnetwork that consists of states that show high activity in postcentral, precentral, superior temporal superior, and white matter areas. The engagement of the two sub-networks is consistent with the cognitive and motor aspects of the PCET task. The area labeled as white matter may consist of axonal fibers connecting these regions and possibly from subcortical areas, which may explain the engagement of the parieto-motor subnetwork.

3.6 Deeper and wider frontal basins in controls, but not in AOS, correlated with higher cognitive scores

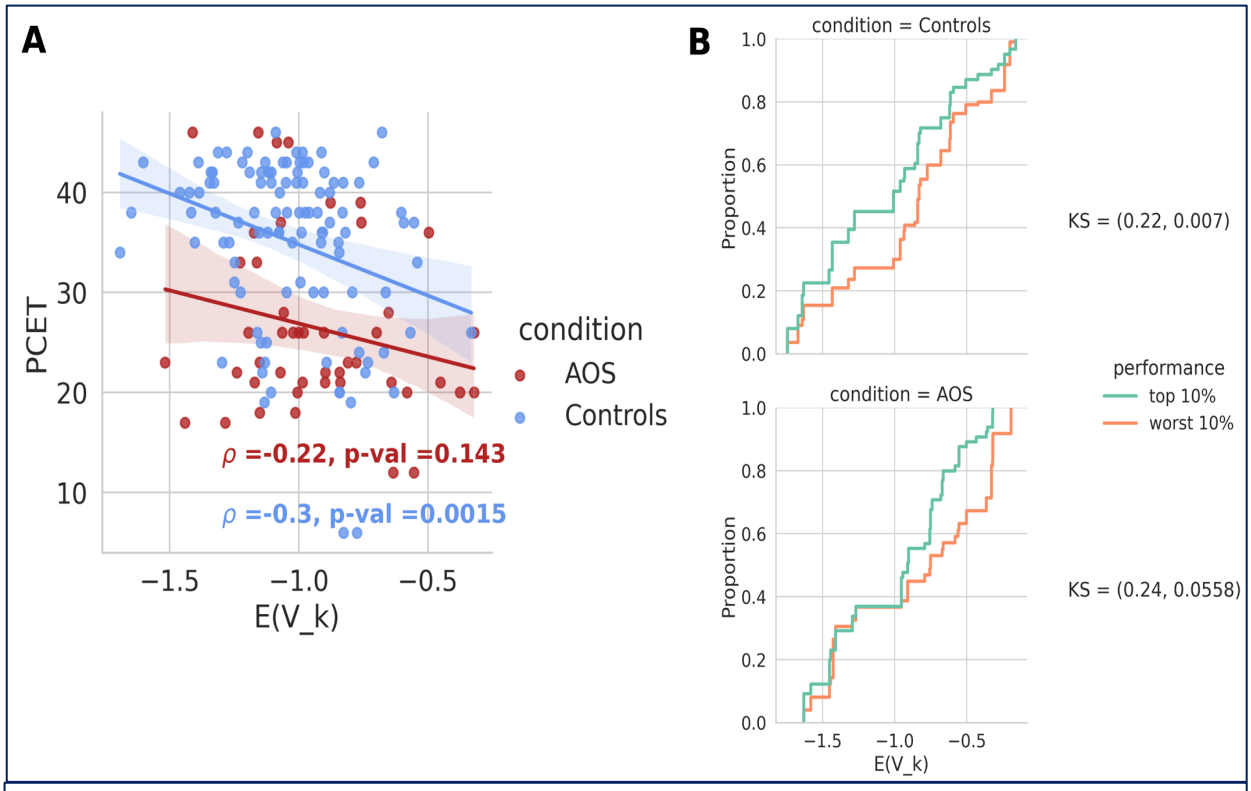

Figure 8: Lower energy of frontal states correlates significantly with higher cognitive score in controls but not in AOS. A) The average energy in frontal states for every subject (control or AOS) was calculated and plotted against the subject's PCET scores. Controls show a significant negative correlation between the frontal energy values and PCET scores (ρ = - 0.3, p = 0.0015), but this relation did not hold for AOS patients (ρ = – 0.22, p = 0.143). B) The cumulative distribution function for the top 10% of performers in the control group shows a significant shift towards low energy states compared to that of the bottom 10% of performers (top, KS: 0.22, p = 0.007), whereas the distributions for AOS conditions show a shift but do not show a significant difference (bottom, KS: 0.24, p = 0.056).

When we limited the analysis of energy values to just the frontal states, we observed a significant negative correlation between the energy values and PCET scores among controls (ρ=—0.3, p=0.0015), suggesting that activation of low-energy frontal states was associated with better cognitive performance among controls. In the AOS group, this relationship was not significant (ρ=—0.22, p=0.14); however, the AOS subjects did show a 30.84% reduction in the basin areas for the frontal states as compared to the controls **(Supplementary Figure 5)**.

We further show the cumulative distribution functions (CDF) of the top 10% and the bottom 10% of performers in both groups **(Figure 8B)**. The CDFs show a clear bias towards lower energies for the top 10% of performers among controls, which differs significantly from the bottom 10% of performers in the control group (KS test, 0.22, p=0.007). The CDFs in the AOS group also featured lower energies for top than bottom performers, but this difference showed a trend toward significance (KS test, 0.24, p=0.06).

3.7 Shallower and high energy basins in AOS correspond to more variable single trial trajectories

We further examined individual trial level trajectories for AOS and healthy controls hypothesizing that deeper basins represent stability in neural dynamics, i.e. similar states are frequently and reliably visited, this should be reflected as lower variability in the single trial trajectories. Consequently, shallower basins representing more unstable neural dynamics should correspond to high variability in the single trial trajectories.

In order to achieve the highest contrast between the groups, we selected top 5 performers from control groups and bottom 5 performers among AOS on the PCET task. The states for these selected subjects were projected on to the PC dimensions and smoothened to derive their energy landscapes **(Figure 9 a, b)**. We observed that the top 5 performers among controls showed deep and low energy basins whereas the bottom 5 performers among AOS showed shallow high energy basins.

The average trial trajectory for every subject consisting of 24 timepoints was averaged over 6 such blocks that a subject visited. These individual trajectories for 5 control and 5 AOS subjects are shown as thin lines in cool and warm colors respectively **(Figure 9 a, b)**.

As can be observed, the trial onsets always corresponded to high energy levels, that switch to lowest energy levels at stimulus onset. At the end of the trials, the dynamics return to the high energy levels. Although there is a clear switch back to higher energy levels way before the trial end, we could not mark this precisely, because the stimulus stayed on all through the trial and different subjects may mentally deem the trial to finish at different times.

The AOS trial trajectories also traverse higher energy levels as compared to controls as expected from their respective energy landscapes. The AOS trial trajectories also show more variability as depicted by the ellipsoid that encompasses the average standard deviation of the spread of trajectories in X (PC1) and Y (PC2) space.

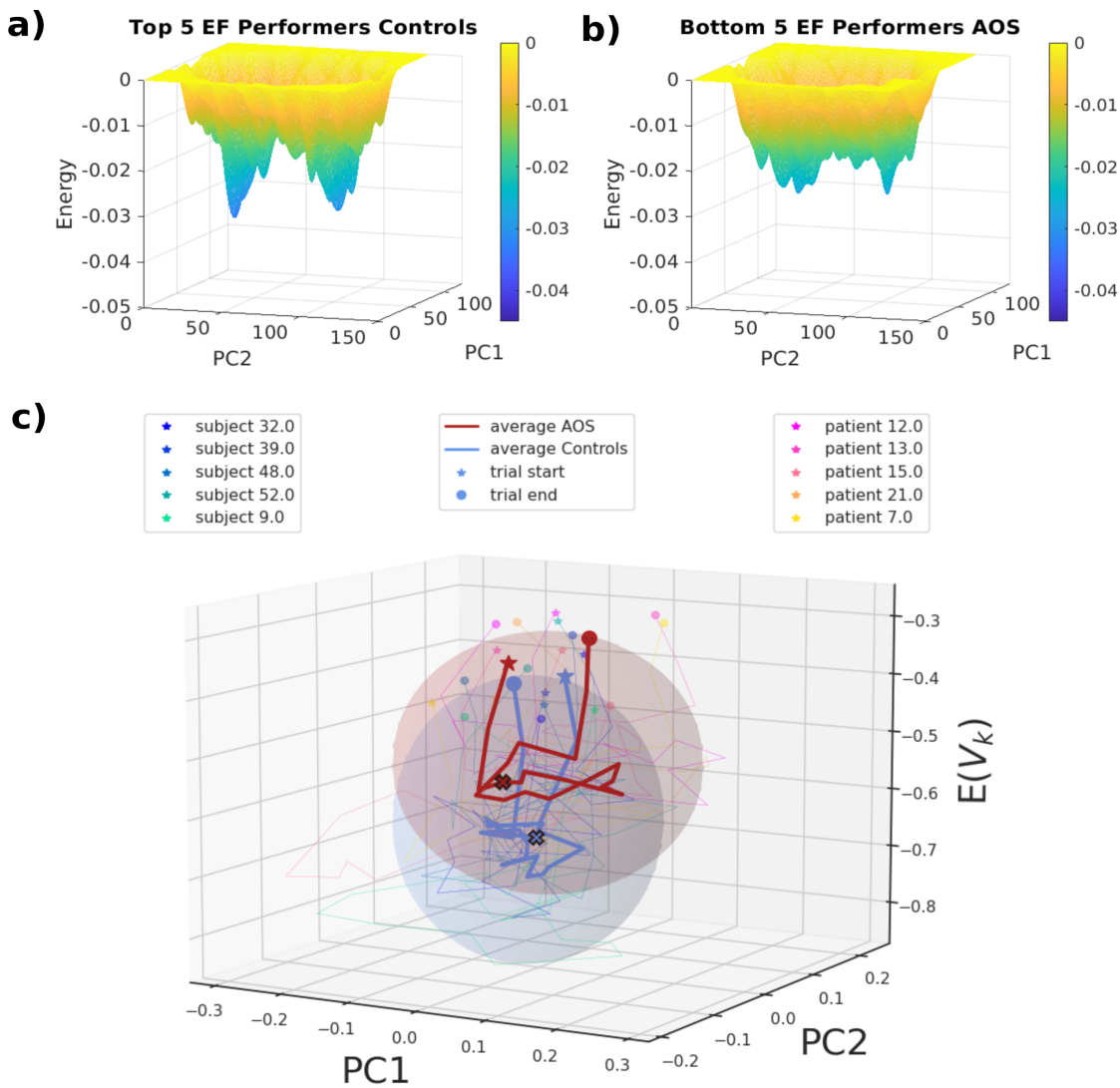

Figure 9: Average single trial trajectories for AOS have more variance compared to Controls: Energy landscapes for top 5 executive function performers in the PCET task for control group (a) and the poorest 5 performers from the AOS group (b). The energy landscape for controls shows deeper basins with lower energy levels compared to AOS. AOS shows shallower basins and higher energy levels. c) Individual average control trajectories are shown in cooler colors and thin lines (blue to green) and individual AOS trajectories are shown in warmer colors (pink to yellow). The star (*) represents the start of the trial and the circle marks the end of a trial. The average trajectory over all 5 individuals for both groups are shown as thick blue lines for controls and as red lines for AOS. The filled X represent the stimulus onset during the trial. The ellipsoid encompasses the average standard deviation across all 5 controls or AOS subject trajectories in X (PC1), Y(PC2) and Z (energy) axes. A higher radius of the ellipsoid along X and Y axis as seen for AOS suggests higher spread for AOS trajectories over PC1 and PC2.

4. Discussion

In this study, we applied for the first time a MEM model to understand the characteristics of energy, an integrated measure of regional activation and coactivation, among AOS and healthy subjects and its relationship to executive function performance. In the context of significantly impaired performance on PCET by the AOS compared to controls, we show that the average energy values across the activation time series for each subject correlate with that subject's PCET accuracy **(Figure 5B)**. This

was observed in the data from the combined sample of AOS and healthy controls as well as at the individual group levels. The relationship showed that the healthy subjects achieved lower energy states more often than AOS and better executive function correlated with lower energy values **(Figure 6A)**, suggesting a less optimized activation-coactivation pattern that may be unfavorable for optimum executive function performance among AOS compared to controls. For example, low energy states occurring with higher probability may represent more stable neural dynamics favoring better cognitive functioning. Further, the PCs of the energy landscape corresponded to the fronto-temporal and parieto-motor networks, where activation of the fronto-temporal network but not the parieto-motor network correlated with executive function performance, highlighting that critical networks underlying cognitive functions can be identified using MEM. The engagement of these two sub-networks is consistent with the cognitive and motor aspects of the PCET task. The area labeled as white matter may consist of axonal fibers connecting these regions and possibly from subcortical areas, which may explain the engagement of the parieto-motor subnetwork. Overall, our findings suggest that the application of MEM to examine functional brain network configuration is a useful strategy.

The utility of the MEM and associated energy is further supported by our finding that first-order activations show only nominal correlations with executive function performance **(Figure 4)** that do not survive multiple test corrections. This result highlights the limitations of regional activation differences in explaining higher level behaviors such as cognitive performance and suggests the need for a more comprehensive mathematical model that combines first and second-order statistics of the data. Our results confirm that MEM model-derived energy values account for a larger variance of performance and that this energy model may be a useful tool for characterizing the putative mechanisms underlying differences in cognition between diagnostic groups since it can be linked with higher level behavior. Since lower energy values occur with higher probability and arise more frequently in controls with better cognitive performance, our analysis suggests that cognitive impairments among AOS may be associated with sub-optimal brain activation-coactivation patterns.

While the average energy across the fMRI activation states attained for an individual correlated with their PCET score, and the PCET scores significantly differed between the clinical groups, the average energy levels over the entire time series for each subject did not differ between the clinical groups **(Fig 5B inset)**. Nonetheless, within a common energy landscape derived jointly for the two groups, clustering states into bins according to their MEM energy suggests that the control group attains more low energy states, and the AOS group spends more time in high energy states **(Figure 6A)**. When energy was plotted over the entire length of fMRI data acquisition during task performance for each subject, we observed that during task blocks, members of the AOS group were more likely to reach high energy states than were control group members (**Figure 6B**). These findings suggest that although the total energy may not be different between the groups, the time course of energy during task performance may be more important. It is possible that the more frequent occurrence of low energy states in individuals with better cognitive performance corresponds to the recognition of a common element across task blocks or reliance on a single successful strategy possibly using evidence accumulation or other processes, whereas the association of higher energy states with poorer performance could correspond to subjects treating each task block as more of a novel challenge and failing to return to and exploit previously successful strategies. When they “solve” the task, they then fall back into a lower, more probable, and more stable state. The

more effort a subject put into "solving" the cognitive task, the higher the energy of the activation-coactivation pattern involved may be. Visiting such states may also relate to making incorrect responses; indeed, such higher energy bins may represent a range of different incorrect strategies or may not represent strategies to solve the cognitive task, but instead reflect a lack of coherent, focused engagement of the task, while the lower energy bins may represent convergent correct strategies, although a caveat of these ideas is that neuronal computation does not happen at the level of BOLD signals.

During the course of the task, all subjects showed two primary energy minima and attraction basins **(Figure 7A)**. PCA shows that these basins corresponded to activation of two distinct sub-networks **(Figure 7C)**, namely the fronto-temporal and parieto-motor, which may correspond to cognitive and motor aspects of this task. The lower the average energy was in the fronto-temporal states, the better the cognitive performance among controls **(Figure 8)**. However, this relationship is lost among AOS, suggesting dysfunction of the fronto-temporal network. A shallowness of basins among AOS, especially in the fronto-temporal network may support longstanding observation of hypofrontality using fMRI [50-52], EEG [53] and PET [54,55] studies. Prior studies supporting hypofrontality relied mainly on first order regional activation differences consisting of decreased activation in the prefrontal regions. Our data extend the finding of hypofrontality to represent brain energy states that include both the first-order activation and second-order coactivation suggesting that hypofrontality includes higher occurrence of unstable high energy states that would correspond to critical prefrontal regions inefficiently participating in executive function processing. This is supported by loss of correlation between basin size of fronto-temporal network and executive function performance in AOS, unlike what is observed in controls, suggesting that the higher occurrence of high energy states of the fronto-temporal network may lead to a loss of the functional link between executive function and fronto-temporal network activation.

The left precentral and right postcentral, both sensory-motor areas, were also represented in the model. A region labeled as white matter, which is located near the left anterior cingulate, was also included in the model although these three regions may have less direct neurocognitive relevance because the region selection step was entirely data-driven. Further, subjects respond to the task prompts using a clickable scroll wheel, which justifies inclusion of sensory-motor regions; not engaging the precentral gyrus for instance means not submitting prompt responses and thus doing poorly. Regarding the white matter region, recent studies show that the vascularization of white matter[49] is relevant for task-related BOLD fMRI analysis[56], given the known role of glia in modulating neuronal signaling[57].

The shallower basins suggest an increase in instability of underlying neural dynamics, i.e. not invoking or visiting the same state reliably, thereby resulting in reduced probability and increased energy levels associated with the state. We hypothesized that the shallower basins should result in more variable single trial trajectories during the task. We indeed found that AOS patients (5 worst performing) not only showed shallow basins **(Figure 9b)** as compared to controls (Figure 9a) but also higher variability in average trajectories for a single trial **(Figure 9c)**.

The results of our study suggest that impaired PCET performance in AOS individuals is related to potentially unfavorable neural dynamics in the fronto-temporal subnetwork consisting of the left olfactory, frontal superior medial, right temporal superior, and frontal superior orbital regions. This is a first-order statistical finding in principle, but due to the nature of multiple comparisons it is difficult to

have confidence in these first-order associations. A second-order finding would contextualize the task-associated regions in a network, usually a covariance network where correlations of time series indicate connection strength, but that could lack temporal specificity if dynamic component is not incorporated. Comparing the strength and smoothness of the correlations in the first-order statistical mappings (**Figure 4A)** to the relationship of the same cognitive variable (PCET score) and the integrated first-and-second-order energy term (**Figure 5B**) indicates the improvement associated with modeling regional coactivation along with individual regional activity using the Ising model. The MEM also reveals that this network has many unequal activation configurations that exist in an energy spectrum where a wide swath of more probable lower energy states is associated with better task performance.

Future research is needed to study full-brain MEMs, for instance using the 360-cortical node Glasser atlas[58] and focus on elucidating trajectories of brain states[59] through an "energy landscape" where basins represent higher probability states that correspond to attractors for the dynamics of neural activity. Our analysis of state frequency by group did not point to any specific states that occur in one group statistically more frequently than in the other group after FDR correction (**Supplemental Figure 3**). With more data, a future step would be to consider subject-level trajectories on the energy landscape defined by the sequence of activation states each subject exhibits during data collection, with possible clustering of trajectories to identify distinct phases and strategies of task performance.

Data availability

The data is available through NIMH data repository.

Acknowledgments

Authors thank Ms. Diana Dworakowski, Ms. Shaelyn Coles, Ms. Lydia Harvey, Mr. Dylan Tomsey, and Ms. Molly Stevens for their efforts in enrolling and characterizing participants. Authors also thank Dr. Matcheri Keshavan MD and Dr. Shaun Eack PhD for arriving at consensus diagnosis on participants after reviewing the clinical evaluations.

Funding Sources

Funding was provided by NIMH grant numbers: R01MH115026 and R01MH112584 (KMP).

Conflicts of Interest:

All authors declare no conflicts of interest associated with this work.

Author Contributions

NT performed analysis and drafted the manuscript; JB created the MEM implementation, performed analysis and participated in editing the manuscript; JR conceptualized the study design, supervised the analysis, and participated in drafting and editing manuscript; BM preprocessed the imaging data; KP managed the enrolment and characterization of participants in the study including obtaining the MRI data, conceptualized the study design, supervised the analysis, and participated in drafting and editing manuscript.

Supplementary Material

S.1 Maximum entropy model (MEM) fits

The MEM fitted to the combined data from control and AOS patients show a good fit to the first-order (mean activity) and second-order (covariance) statistics of the data.

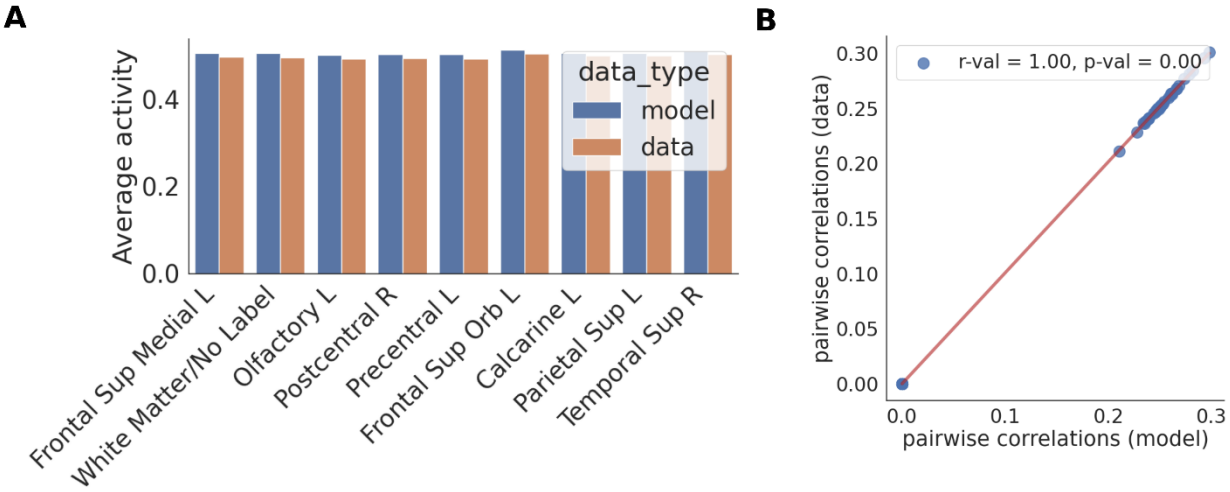

Supplemental Figure 1: Goodness of fit of first-order and second-order statistics

S.2. Theoretical Versus Empirical Probability

Comparing the predicted (theoretical) probability of state occurrence by the MEM to the energy of the same states shows a strict, zero-variance monotonically increasing relationship, as expected (top of Supplemental **Figure 2)**. Comparing this same energy term to the observed (empirical) frequency (in the concatenated binary matrix, T) of the same states (bottom of Supplemental **Figure P**) can be considered a goodness of fit test. While the MEM is internally tested for goodness of fit, this result confirms that the model is capturing differences in state occurrence frequency. Moreover, it is a direct illustration of the relationship between energy and probability. Note that the empirical probabilities are what the model used to fit, so this result only indicates that the fitting succeeded.

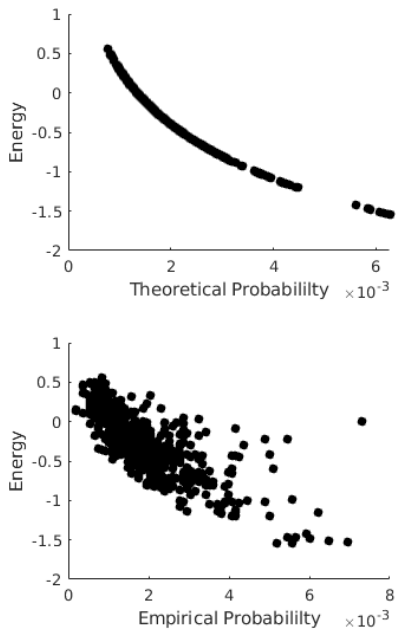

Supplementary Figure 2. Top: the energy and probability terms from the model. Bottom: the energy term from the model versus the actual empirical probabilities of the same states.

S.3. States by Group without Considering Energy

Attempting to look for differences in occurrence frequency of specific states (without binning them by energy) by group did not yield any significant difference after FDR correction when a two-sample t-test was used to compare the frequency of visits to specific states among individuals by group.

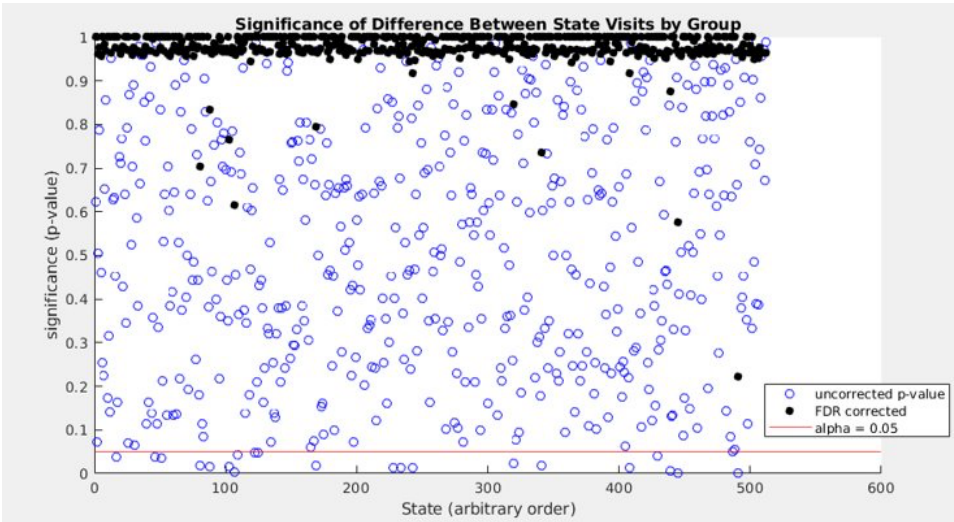

Supplemental Figure 3. Differences in State Occurrence by Group. The x-axis lists states in an arbitrary order. The y-axis provides the significance, by two-sample t-test, between the number of visits across subjects for the given state between groups. The horizontal line indicates an alpha cutoff for significance of 0.05. While a few states are marginally significant before FDR correction, no specific states occur at significantly different frequencies by group after FDR.

S.4. Standard Deviations of Energy Bin over Time

Because the groups have different sizes, it is possible that the results in **Figure 4** are driven by differences in the variances of the groups. This is not the case. The groups have standard deviations that are statistically not significant by KS-test.

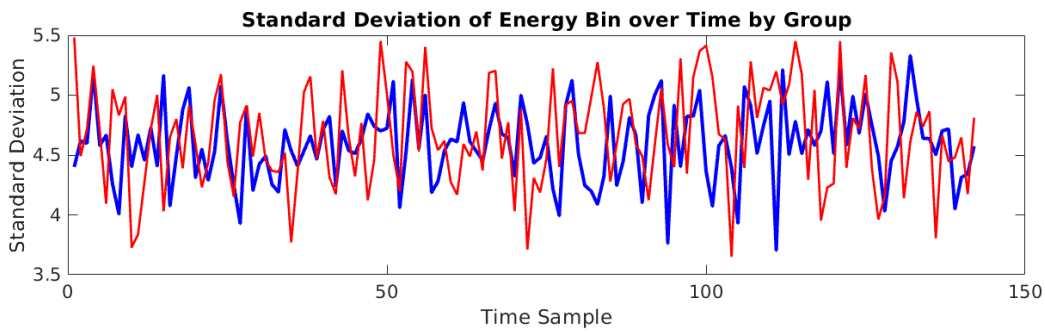

Supplemental Figure 4. Standard Deviation of Energy Bin over Time by Group. X-axis: time (one sample is 3 seconds). Y-axis: standard deviation of energy bin assignment across subjects within a group at a given time point. Blue: controls; red: AOS.

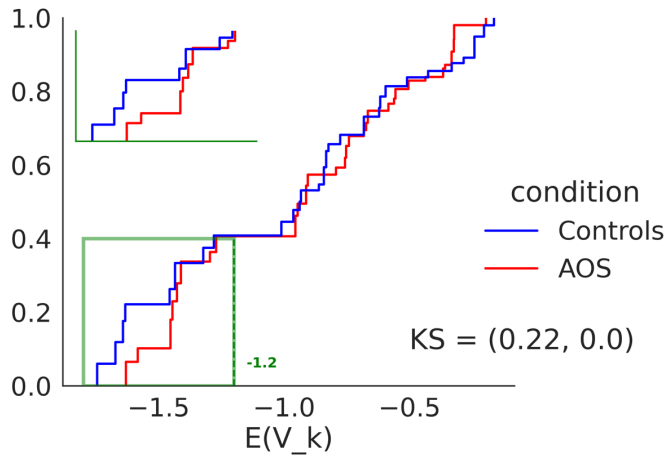

Supplemental Figure 5. Cumulative distribution over energy of only the frontal states for Controls and AOS. The AOS patients show a 30.84% reduction in the basin area in frontal states as compared to the Controls.

REFERENCES

1 Frangou, S. Cognitive function in early onset schizophrenia: a selective review. *Frontiers in human neuroscience* **3**, 79, doi:10.3389/neuro.09.079.2009 (2010).

2 Kumra, S., Shaw, M., Merka, P., Nakayama, E. & Augustin, R. Childhood-onset schizophrenia: research update. *Canadian journal of psychiatry. Revue canadienne de psychiatrie* **46**, 923-930 (2001).

3 Rapoport, J. L. *et al.* Childhood-onset schizophrenia. Progresive ventricular change during adolescence. *Archives of general psychiatry* **54**, 897-903 (1997).

4 Kumra, S. & Charles Schulz, S. Editorial: research progress in early-onset schizophrenia. *Schizophrenia bulletin* **34**, 15-17, doi:sbm123 [pii]; 10.1093/schbul/sbm123 (2008).

5 Holtmaat, A. & Svoboda, K. Experience-dependent structural synaptic plasticity in the mammalian brain. *Nature reviews. Neuroscience* **10**, 647-658, doi:10.1038/nrn2699 (2009).

6 Kester, H. M. *et al.* Decision-making impairments in adolescents with early-onset schizophrenia. *Schizophrenia research* **85**, 113-123, doi:S0920-9964(06)00102-2 [pii]; 10.1016/j.schres.2006.02.028 (2006).

7 Thaden, E. *et al.* Early-onset schizophrenia is associated with impaired adolescent development of attentional capacity using the identical pairs continuous performance test. *Schizophrenia research* **81**, 157-166, doi:10.1016/j.schres.2005.09.015 (2006).

8 Brickman, A. M. *et al.* Neuropsychological functioning in first-break, never-medicated adolescents with psychosis. *J Nerv Ment Dis* **192**, 615-622 (2004).

9 White, T., Mous, S. & Karatekin, C. Memory-guided saccades in youth-onset psychosis and attention deficit hyperactivity disorder (ADHD). *Early intervention in psychiatry*, doi:10.1111/eip.12038 (2013).

10 Karatekin, C., Bingham, C. & White, T. Regulation of cognitive resources during an n-back task in youth-onset psychosis and attention-deficit/hyperactivity disorder (ADHD). *International journal of psychophysiology : official journal of the International Organization of Psychophysiology* **73**, 294-307, doi:10.1016/j.ijpsycho.2009.05.001 (2009).

11 Karatekin, C., White, T. & Bingham, C. Divided attention in youth-onset psychosis and attention deficit/hyperactivity disorder. *Journal of abnormal psychology* **117**, 881-895, doi:10.1037/a0013446 (2008).

12 Oie, M. & Rund, B. R. Neuropsychological deficits in adolescent-onset schizophrenia compared with attention deficit hyperactivity disorder. *The American journal of psychiatry* **156**, 1216-1222 (1999).

13 Oie, M., Sundet, K. & Rund, B. R. Neurocognitive decline in early-onset schizophrenia compared with ADHD and normal controls: evidence from a 13-year follow-up study. *Schizophrenia bulletin* **36**, 557-565, doi:10.1093/schbul/sbn127 (2010).

14 Woodward, N. D., Purdon, S. E., Meltzer, H. Y. & Zald, D. H. A meta-analysis of neuropsychological change to clozapine, olanzapine, quetiapine, and risperidone in schizophrenia. *The international journal of neuropsychopharmacology / official scientific journal of the Collegium Internationale Neuropsychopharmacologicum* **8**, 457-472, doi:S146114570500516X [pii]; 10.1017/S146114570500516X (2005).

15 Mishara, A. L. & Goldberg, T. E. A meta-analysis and critical review of the effects of conventional neuroleptic treatment on cognition in schizophrenia: opening a closed book. *Biological psychiatry* **55**, 1013-1022, doi:10.1016/j.biopsych.2004.01.027 (2004).

16 Bora, E., Gokcen, S., Kayahan, B. & Veznedaroglu, B. Deficits of social-cognitive and social-perceptual aspects of theory of mind in remitted patients with schizophrenia: effect of residual symptoms. *J Nerv Ment Dis* **196**, 95-99 (2008).

17 Frith, C. Neuropsychology of schizophrenia, what are the implications of intellectual and experiential abnormalities for the neurobiology of schizophrenia? *Br Med Bull* **52**, 618-626. (1996).
18 Green, M. F. What are the functional consequences of neurocognitive deficits in schizophrenia? *The American journal of psychiatry* **153**, 321-330 (1996).
19 Velligan, D. I. & Miller, A. L. Cognitive dysfunction in schizophrenia and its importance to outcome: the place of atypical antipsychotics in treatment. *The Journal of clinical psychiatry* **60 Suppl 23**, 25-28 (1999).
20 Gitelman, D. R., Penny, W. D., Ashburner, J. & Friston, K. J. Modeling regional and psychophysiologic interactions in fMRI: the importance of hemodynamic deconvolution. *NeuroImage* **19**, 200-207, doi:10.1016/s1053-8119(03)00058-2 (2003).
21 Worsley, K. J., Evans, A. C., Marrett, S. & Neelin, P. A three-dimensional statistical analysis for CBF activation studies in human brain. *Journal of cerebral blood flow and metabolism : official journal of the International Society of Cerebral Blood Flow and Metabolism* **12**, 900-918, doi:10.1038/jcbfm.1992.127 (1992).
22 Friston, K. J. *et al.* Statistical parametric maps in functional imaging: A general linear approach. *Human brain mapping* **2**, 189-210, doi:10.1002/hbm.460020402 (1994).
23 Yeh, F. C. *et al.* Maximum Entropy Approaches to Living Neural Networks. *Entropy* **12**, 89-106, doi:10.3390/e12010089 (2010).
24 Schneidman, E. Towards the design principles of neural population codes. *Current Opinion in Neurobiology* **37**, 133-140, doi:https://doi.org/10.1016/j.conb.2016.03.001 (2016).
25 Kloucek, M. B. *et al.* Biases in inverse Ising estimates of near-critical behavior. *Phys Rev E* **108**, 014109, doi:10.1103/PhysRevE.108.014109 (2023).
26 Das, T. K. *et al.* Highlighting the structure-function relationship of the brain with the Ising model and graph theory. *Biomed Res Int* **2014**, 237898, doi:10.1155/2014/237898 (2014).
27 Kang, J., Jeong, S. O., Pae, C. & Park, H. J. Bayesian estimation of maximum entropy model for individualized energy landscape analysis of brain state dynamics. *Human brain mapping* **42**, 3411-3428, doi:10.1002/hbm.25442 (2021).
28 Brush, S. G. History of the Lenz-Ising Model. *Reviews of Modern Physics* **39**, 883-893, doi:10.1103/RevModPhys.39.883 (1967).
29 Ezaki, T., Fonseca Dos Reis, E., Watanabe, T., Sakaki, M. & Masuda, N. Closer to critical resting-state neural dynamics in individuals with higher fluid intelligence. *Commun Biol* **3**, 52, doi:10.1038/s42003-020-0774-y (2020).
30 Kang, J., Pae, C. & Park, H. J. Energy landscape analysis of the subcortical brain network unravels system properties beneath resting state dynamics. *NeuroImage* **149**, 153-164, doi:10.1016/j.neuroimage.2017.01.075 (2017).
31 Watanabe, T. *et al.* Energy landscapes of resting-state brain networks. *Frontiers in neuroinformatics* **8**, 12, doi:10.3389/fninf.2014.00012 (2014).
32 Gold, J. M. *et al.* Selective Attention, Working Memory, and Executive Function as Potential Independent Sources of Cognitive Dysfunction in Schizophrenia. *Schizophrenia bulletin* **44**, 1227-1234, doi:10.1093/schbul/sbx155 (2018).
33 Jepsen, J. R. *et al.* Deficient maturation of aspects of attention and executive functions in early onset schizophrenia. *European child & adolescent psychiatry* **19**, 773-786, doi:10.1007/s00787-010-0126-4 (2010).
34 Johnson-Selfridge, M. & Zalewski, C. Moderator variables of executive functioning in schizophrenia: meta- analytic findings. *Schizophrenia bulletin* **27**, 305-316 (2001).

35 Minzenberg, M. J., Laird, A. R., Thelen, S., Carter, C. S. & Glahn, D. C. Meta-analysis of 41 functional neuroimaging studies of executive function in schizophrenia. *Archives of general psychiatry* **66**, 811-822, doi:66/8/811 [pii]; 10.1001/archgenpsychiatry.2009.91 (2009).
36 Gur, R. C. *et al.* Computerized neurocognitive scanning: II. The profile of schizophrenia. *Neuropsychopharmacology : official publication of the American College of Neuropsychopharmacology* **25**, 777-788 (2001).
37 Gur, R. C. *et al.* Computerized neurocognitive scanning: I. Methodology and validation in healthy people. *Neuropsychopharmacology : official publication of the American College of Neuropsychopharmacology* **25**, 766-776 (2001).
38 **Prasad, K. M.** *et al.* RGS4 polymorphisms associated with variability of cognitive performance in a family-based schizophrenia sample. *Schizophrenia bulletin* **36**, 983-990, doi:10.1093/schbul/sbp002 (2010).
39 **Prasad, K. M.**, Muldoon, B., Theis, N., Iyengar, S. & Keshavan, M. S. Multipronged investigation of morphometry and connectivity of hippocampal network in relation to risk for psychosis using ultrahigh field MRI. *Schizophrenia research* **256**, 88-97, doi:10.1016/j.schres.2023.05.002 (2023).
40 Roalf, D. R. *et al.* Neurocognitive performance stability in a multiplex multigenerational study of schizophrenia. *Schizophrenia bulletin* **39**, 1008-1017, doi:10.1093/schbul/sbs078 (2013).
41 Kuo, S. S. *et al.* Cognition and community functioning in schizophrenia: The nature of the relationship. *Journal of abnormal psychology* **127**, 216-227, doi:10.1037/abn0000326 (2018).
42 Kurtz, M. M., Wexler, B. E. & Bell, M. D. The Penn Conditional Exclusion Test (PCET): relationship to the Wisconsin Card Sorting Test and work function in patients with schizophrenia. *Schizophrenia research* **68**, 95-102, doi:10.1016/S0920-9964(03)00179-8 (2004).
43 Esteban, O. *et al.* fMRIPrep: a robust preprocessing pipeline for functional MRI. *Nature methods* **16**, 111-116, doi:10.1038/s41592-018-0235-4 (2019).
44 Glasser, M. F. *et al.* The minimal preprocessing pipelines for the Human Connectome Project. *NeuroImage* **80**, 105-124, doi:10.1016/j.neuroimage.2013.04.127 (2013).
45 Varoquaux, G. *et al.* A group model for stable multi-subject ICA on fMRI datasets. *NeuroImage* **51**, 288-299, doi:10.1016/j.neuroimage.2010.02.010 (2010).
46 Salman, M. S., Vergara, V. M., Damaraju, E. & Calhoun, V. D. Decreased Cross-Domain Mutual Information in Schizophrenia From Dynamic Connectivity States. *Front Neurosci* **13**, 873, doi:10.3389/fnins.2019.00873 (2019).
47 Allen, E. A. *et al.* Tracking whole-brain connectivity dynamics in the resting state. *Cereb Cortex* **24**, 663-676, doi:10.1093/cercor/bhs352 (2014).
48 Zhu, M. & Ghodsi, A. Automatic dimensionality selection from the scree plot via the use of profile likelihood. *Computational Statistics & Data Analysis* **51**, 918-930, doi:10.1016/j.csda.2005.09.010 (2006).
49 Smirnov, M., Destrieux, C. & Maldonado, I. L. Cerebral white matter vasculature: still uncharted? *Brain : a journal of neurology* **144**, 3561-3575, doi:10.1093/brain/awab273 (2021).
50 Carter, C. S. *et al.* Functional hypofrontality and working memory dysfunction in schizophrenia. *The American journal of psychiatry* **155**, 1285-1287. (1998).
51 Glahn, D. C. *et al.* Beyond hypofrontality: a quantitative meta-analysis of functional neuroimaging studies of working memory in schizophrenia. *Human brain mapping* **25**, 60-69, doi:10.1002/hbm.20138 (2005).
52 Callicott, J. H. *et al.* Complexity of prefrontal cortical dysfunction in schizophrenia: more than up or down. *The American journal of psychiatry* **160**, 2209-2215 (2003).
53 Mientus, S. *et al.* Cortical hypoactivation during resting EEG in schizophrenics but not in depressives and schizotypal subjects as revealed by low resolution electromagnetic tomography (LORETA). *Psychiatry research* **116**, 95-111, doi:10.1016/s0925-4927(02)00043-4 (2002).

54 Buchsbaum, M. S. & Wu, J. C. Hypofrontality in schizophrenia as assessed by PET. *The American journal of psychiatry* **144**, 122-123, doi:10.1176/ajp.144.1.aj1441122 (1987).
55 Weinberger, D. R. Implications of normal brain development for the pathogenesis of schizophrenia. *Archives of general psychiatry* **44**, 660-669. (1987).
56 Li, M., Newton, A. T., Anderson, A. W., Ding, Z. & Gore, J. C. Characterization of the hemodynamic response function in white matter tracts for event-related fMRI. *Nat Commun* **10**, 1140, doi:10.1038/s41467-019-09076-2 (2019).
57 Fields, R. D., Woo, D. H. & Basser, P. J. Glial Regulation of the Neuronal Connectome through Local and Long-Distant Communication. *Neuron* **86**, 374-386, doi:10.1016/j.neuron.2015.01.014 (2015).
58 Glasser, M. F. *et al.* A multi-modal parcellation of human cerebral cortex. *Nature* **536**, 171-178, doi:10.1038/nature18933 (2016).
59 Transtrum, M. K. & Qiu, P. Bridging Mechanistic and Phenomenological Models of Complex Biological Systems. *PLoS Comput Biol* **12**, e1004915, doi:10.1371/journal.pcbi.1004915 (2016).